APPLIED SCIENCES AND ENGINEERING

Combinatorial screen of dynamic mechanical stimuli for predictive control of MSC mechano-responsiveness

Haijiao Liu[1,2,3†], Jenna F. Usprech[2,3‡], Prabu Karthick Parameshwar[2,3§], Yu Sun[1,2]*, Craig A. Simmons[1,2,3]*

Mechanobiological-based control of mesenchymal stromal cells (MSCs) to facilitate engineering and regeneration of load-bearing tissues requires systematic investigations of specific dynamic mechanical stimulation protocols. Using deformable membrane microdevice arrays paired with combinatorial experimental design and modeling, we probed the individual and integrative effects of mechanical stimulation parameters (strain magnitude, rate at which strain is changed, and duty period) on myofibrogenesis and matrix production of MSCs in three-dimensional hydrogels. These functions were found to be dominantly influenced by a previously unidentified, higher-order interactive effect between strain magnitude and duty period. Empirical models based on our combinatorial cue-response data predicted an optimal loading regime in which strain magnitude and duty period were increased synchronously over time, which was validated to most effectively promote MSC matrix production. These findings inform the design of loading regimes for MSC-based engineered tissues and validate a broadly applicable approach to probe multifactorial regulating effects of mechanobiological cues.

INTRODUCTION

Mechanical stimulation potently promotes the growth and maturation of tissues (*1*, *2*) and is frequently applied when engineering load-bearing tissues to achieve functional mechanical properties (*3*–*5*). In many native and engineered connective and cardiovascular tissues, mechanically stimulated tissue production results from the mechano-responsiveness of mesenchymal cells, including multipotent mesenchymal stromal cells (MSCs) as a source for engineered tissues (*1*, *6*–*8*). Improved understanding of the effects of dynamic mechanical stimulation on the regulation of MSC fate and functions is required for more effective and efficient cell-based therapies aimed at regeneration of load-bearing tissues (*9*–*11*).

The native mechanical microenvironment of MSCs is inherently complex and includes multiple mechanical factors that are coordinated for delicate regulation of MSC functions (*6*, *10*). Systematic and combinatorial approaches, where multiple mechanical stimuli and factors are included and changed in concert, offer more predictive control over MSC mechano-responses. Multifactorial experimental design and analyses are advantageous in revealing nonlinear and nonintuitive interactions between the factors screened (*12*–*14*). To date, mechanobiological-based control of MSCs to, for example, maximize matrix production toward functional tissues (*2*) has been largely based on best guesses and one-factor-at-a-time approaches, which fail to capture the complex interplay between each factor (i.e., antagonism or synergism). Therefore, more systematic and combinatorial investigations of the effect of complex dynamic mechanical stimulation protocols are required to screen and predict mechanobiological responses of MSCs but have been lacking (*15*, *16*). In particular, although mechanical stimulation parameters like strain magnitude (STRAIN) (*15*), the rate of strain change (RATE) (*3*), and duty period (DUTY) (*17*, *18*) have been explored individually, their interactions and integrative effects on MSC fate and functions, as required to generate guidelines applicable to engineered tissues, have not (*1*, *3*, *19*).

Conventional experimental approaches and platforms are limited in their capability to design and implement combinatorial investigations of dynamic mechanical stimulation protocols. Biomaterial array platforms have been developed to enable systematic investigations of complex cue-response networks with multivariate control of the cellular microenvironment (*14*, *20*–*22*). However, few biomaterial array platforms have integrated mechanical stimulation for mechanobiology studies, despite the critical regulatory effects of mechanical stimulation on cell and tissue functions (*6*). To address this limitation, we and others have previously developed deformable membrane array platforms to study the mechanobiological responses of cells to combinations of environmental cues in two dimensions (*23*, *24*). The deformable membrane platforms that we developed and the stretchable substrate array platforms that others developed have also been adapted to enable three-dimensional (3D) mechanical stimulation of cell-seeded biomaterial constructs (*25*–*27*).

Here, we use a combinatorial experimental approach by pairing microdevice arrays with parametric modeling to identify specific combinations of mechanical loading factors that best promote myofibrogenesis and collagen production of MSCs. We report that MSC mechano-responsiveness is dominated by a novel interaction between strain magnitude and duty period (STRAIN*DUTY). Empirical models based on our combinatorial cue-response data predicted an unexpected optimal loading regime in which strain magnitude and duty period were increased synchronously over time, which was

[1]Department of Mechanical and Industrial Engineering, University of Toronto, Toronto, ON M5S 3G8, Canada. [2]Institute of Biomedical Engineering, University of Toronto, Toronto, ON M5S 3G9, Canada. [3]Translational Biology and Engineering Program, Ted Rogers Centre for Heart Research, Toronto, ON M5G 1M1, Canada.
*Corresponding author. Email: sun@mie.utoronto.ca (Y.S.); c.simmons@utoronto.ca (C.A.S.)
†Present address: Department of Bioengineering, University of Pennsylvania, 210 South 33rd Street, 315S Skirkanich Hall, Philadelphia, PA 19104, USA.
‡Present address: School of Biomedical Engineering, The University of British Columbia, Vancouver Campus, Biomedical Research Centre, 2222 Health Sciences Mall, Room 254, Vancouver, BC V6T 1Z3, Canada.
§Present address: Department of Biological and Biomedical Engineering, McGill University, Duff Medical Building, 3775 Rue University, Room 316, Montréal, QC H3A 2B4, Canada.

confirmed to maximally promote collagen production by MSCs. Thus, the unique combinatorial capabilities of our platform and approach generated novel insights otherwise not available, leading to the identification of a novel mechanical loading regiment for MSC-based tissue engineering. Our findings also validated this broadly applicable approach to systematically identify combinations of mechanical, biomaterial, and other mechanobiological cues that optimally guide cell functions in context-specific niches.

RESULTS

Combinatorial mechanical stimulation of cell-laden hydrogel constructs

Deformable membrane devices were fabricated to house arrays of optically patterned and covalently bound poly(ethylene glycol)-norbornene (PEG-NB) hydrogels (Fig. 1A and fig. S1A). Permutations of rate of strain change (RATE or R in condition acronyms), initial strain magnitude (STRAIN or ε), and duty period (DUTY or D) were imposed to the MSC-laden gels throughout the culture period (Fig. 1B and table S1). Covalent bonding between the gels and substrate membrane transmitted the cyclic deformation and generated up to 16% nominal tensile strain in the gels (Fig. 1C and movie S1). Fluorescent images of cells were acquired and reconstructed into 3D surfaces for the analysis of cell differentiation and matrix production (Fig. 1D). The fluorescent surfaces were batch processed for defined metrics, which were then modeled using least squares estimation and parametric regression techniques (table S2).

Interaction between strain magnitude and duty period dominated MSC mechano-responsiveness

As a model, we studied mechanically stimulated matrix production and myofibroblast differentiation, since myofibroblasts are the critical effectors of tissue remodeling under normal development, repair, and fibrotic conditions (*28*–*30*). Since the formation of α–smooth muscle actin (α-SMA) stress fiber is the hallmark of myofibroblast differentiation (Fig. 2, A and I, and fig. S1B) (*31*), we first analyzed the proportion of α-SMA stress fiber–positive cells (SMA+ proportion) in response to the individual and interactive effects of strain change rate, magnitude, and duty period over 1 week of mechanical stimulation. The quantification of SMA+ proportion across the combinatorial condition patterns (fig. S2A) was used to generate the parametric model of these mechanical factors. While the individual factors each had significant effects, parametric analysis on SMA+ cells revealed that the strain magnitude*duty period interaction had the largest effect (Fig. 2B and table S2), indicating that combining strain magnitude and duty period both at low or high levels [i.e., positive interactions in patterns ($R^{hi}\varepsilon^{lo}D^{lo}$) and ($R^{hi}\varepsilon^{hi}D^{hi}$)] led to a high proportion of SMA+ cells (red in Fig. 2C and fig. S3A; Fig. 2I). In contrast, mismatched levels of strain magnitude and duty period [e.g., pattern ($R^{lo}\varepsilon^{lo}D^{hi}$) in Fig. 2I] or their negative interaction led to low SMA+ proportion (blue in Fig. 2C and fig. S3A). Although no significant change in cell density was observed across the loading patterns (fig. S4A), mechanical stimulation not only increased spreading in MSCs (Fig. 2I and fig. S1B) but also increased the expression of collagen at local cell protrusions and edges (rim of cell in Fig. 2, D and I, zoom-in) compared to those in static culture. Cells that stained for collagen were defined as "collagen positive" (Col+). Similarly, the quantification of Col+ proportion and collagen intensity across the combinatorial condition patterns (fig. S2, B and C) was used to generate the parametric models. The parametric analysis on Col+ proportion and collagen intensity consistently revealed the strain magnitude*duty period interaction as the most sizeable effect (Fig. 2, E and G). Combining strain magnitude and duty period both at low or high levels, i.e., positive strain magnitude*duty period [e.g., patterns ($R^{hi}\varepsilon^{lo}D^{lo}$) and ($R^{hi}\varepsilon^{hi}D^{hi}$)], led to high Col+ proportion and collagen intensity (red in Fig. 2, F and H, and fig. S3, B and C), while mismatched levels of strain magnitude and duty period, i.e., negative strain magnitude*duty period [e.g., patterns ($R^{lo}\varepsilon^{lo}D^{hi}$) and ($R^{lo}\varepsilon^{hi}D^{lo}$)], led to low collagen production (blue in Fig. 2, F and H, and fig. S3, B and C).

Harnessing the interactive effect of strain magnitude*duty period is hypothesized to enhance matrix production by MSCs

Hit conditions were selected for longer-term validation

For engineered load-bearing tissues, mechanical stimulation is typically applied more than 1 week to promote tissue growth. Therefore, we sought to confirm whether selected hit conditions for collagen production from 1 week of culture could maintain their longer-term effects. To comprehensively assess the collagen production from all cells and to avoid potentially biased quantification due to MSC heterogeneity (such as high mean intensity from a small population of brightly stained cells), a new metric "weighted collagen" (wCol) was defined that accounted for both the population of collagen-producing cells based on Col+ proportion and the average level of collagen production based on mean fluorescent intensity (see Materials and Methods). The wCol sensitivity test indicated no significant effect of the weight variation to Col+ proportion and collagen intensity on all conditions tested (fig. S5) and on the wCol surface response model (fig. S6), and thus, we chose the equal weight assignment as the representation for all the analyses hereafter. All conditions were evaluated for levels of wCol to identify the optimal, medial, and pessimal conditions of collagen production (Fig. 2J and figs. S5A and S6, left). Patterns ($R^{hi}\varepsilon^{lo}D^{lo}$), ($R^{mid}\varepsilon^{mid}D^{mid}$), and ($R^{lo}\varepsilon^{hi}D^{lo}$) that respectively produced the greatest wCol (95/100; Fig. 2, I and L), the medial level wCol (50/100; Fig. 2, I and K), and the lowest wCol (13/100; Fig. 2, I and J) were selected for further validation with extended 2-week culture. Notably, the individual effect of strain change rate (RATE) and the interactive effect of strain magnitude*duty period (STRAIN*DUTY) were both significant and positive for all metrics evaluated (Fig. 2 and fig. S7). In particular, the strain magnitude*duty period interaction had its maximal effect for both SMA and collagen expression at high rate of strain change of 1%/2 days (diagonal distribution of red in Fig. 2, C, F, H, and L, and fig. S3). This is because the positive effects of rate of strain change and strain magnitude*duty period were additive. In contrast, the effects of other factors such as strain magnitude and rate of strain change*duty period were mostly inconsistent and/or insignificant. Therefore, additional conditions at high rate of strain change of 1%/2 days [i.e., patterns ($R^{hi}\varepsilon^{hi}D^{hi}$), ($R^{hi}\varepsilon^{lo}D^{hi}$), and ($R^{hi}\varepsilon^{hi}D^{lo}$)] were selected and added to the pattern ($R^{hi}\varepsilon^{lo}D^{lo}$) to form a full factorial design to validate the above identified effect of strain magnitude*duty period interaction on MSC responses (Fig. 2L). Final conditions selected for the 2-week validation culture are listed in table S3.

*Strain magnitude*duty period dominantly affects myofibroblast differentiation and matrix production after 2 weeks of culture*

Each metric analyzed was quantified across the selected conditions for validation to generate the new parametric models (fig. S8). Prediction expressions of the parametric models are shown in table

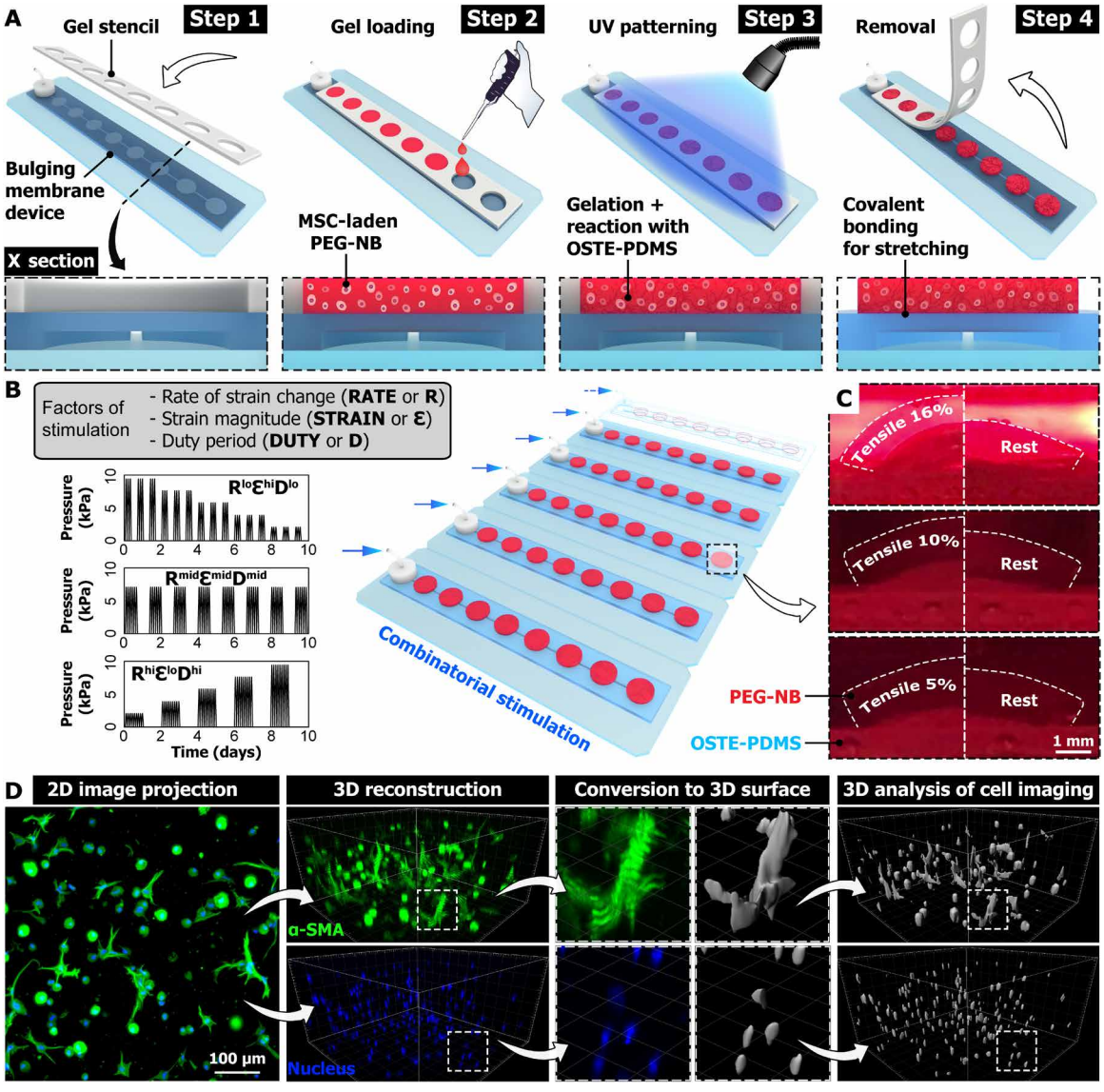

Fig. 1. Combinatorial mechanical stimulation of cell-laden hydrogel constructs. (**A**) Engineered hydrogel construct arrays are optically patterned and covalently bound to microdevice arrays with deformable membranes, to allow 3D mechanical stretching of cells seeded in the gels. (**B**) Examples of actuation pressure profile to achieve combinatorial mechanical stimulation patterns in combination of defined levels of rate of strain change (RATE or R), strain magnitude (STRAIN or ε), and duty period (DUTY or D). (**C**) Side view of PEG-NB gels in culture deformed by the membrane under the prescribed actuation pressure, achieving 16, 10, and 5% of nominal tensile strain. For comparison, the right half image of each group (white dashed line) shows the same gel at rest. (**D**) For each laser channel (e.g., SMA in green and nucleus in blue), 3D surfaces are generated using 3D image reconstruction (images in isometric view) and automatic thresholding in Imaris (gray). The parametric analysis on various metrics from the fluorescent images and surfaces are performed to assess mechanobiological responses of MSCs (e.g., myofibroblast differentiation and matrix production). UV, ultraviolet; OSTE-PDMS, off-stoichiometry thiol-ene based polydimethylsiloxane.

S4. While no significant change in the cell density across the loading patterns and initial seeding density was observed by 2 weeks (fig. S4B), the SMA+ proportion was generally increased in comparison to that by 1 week, particularly with significant increase in patterns ($R^{mid}\varepsilon^{mid}D^{mid}$), ($R^{hi}\varepsilon^{lo}D^{lo}$), and ($R^{hi}\varepsilon^{hi}D^{hi}$) (fig. S2A). Parametric analysis of SMA+ proportion revealed that, by 2 weeks (Fig. 3, A and B), the strain magnitude*duty period interaction was still positive and had the greatest effect (Fig. 3C and table S4), generating a saddle-shaped response surface (Fig. 3D). The SMA+ proportion increased with strain magnitude and duty period both at high and low levels (red in Fig. 3D) and peaked at 19.1% with rate of strain change, strain magnitude, and duty period at 1%/2 days, 4%, and 3 hours ON/OFF [i.e., pattern ($R^{hi}\varepsilon^{lo}D^{lo}$) in Fig. 3B and fig. S9]. To complement SMA+ as a marker of myofibroblasts, we also analyzed the expression of fibronectin as an early indicator of activation of myofibroblasts (*32*–*34*). Similar to SMA+, fibronectin intensity increased with positive strain magnitude*duty period interaction [Fig. 3, E and red in F; pattern ($R^{hi}\varepsilon^{hi}D^{hi}$) in Fig. 3B and figs. S8B and S9]. In contrast, mismatched levels of strain magnitude and duty period inhibited both SMA+ proportion and fibronectin intensity (blue in Fig. 3, D and F; pattern ($R^{hi}\varepsilon^{hi}D^{lo}$) in Fig. 3B and fig. S9). Similarly by 2 weeks, the Col+ proportion and collagen intensity were significantly increased

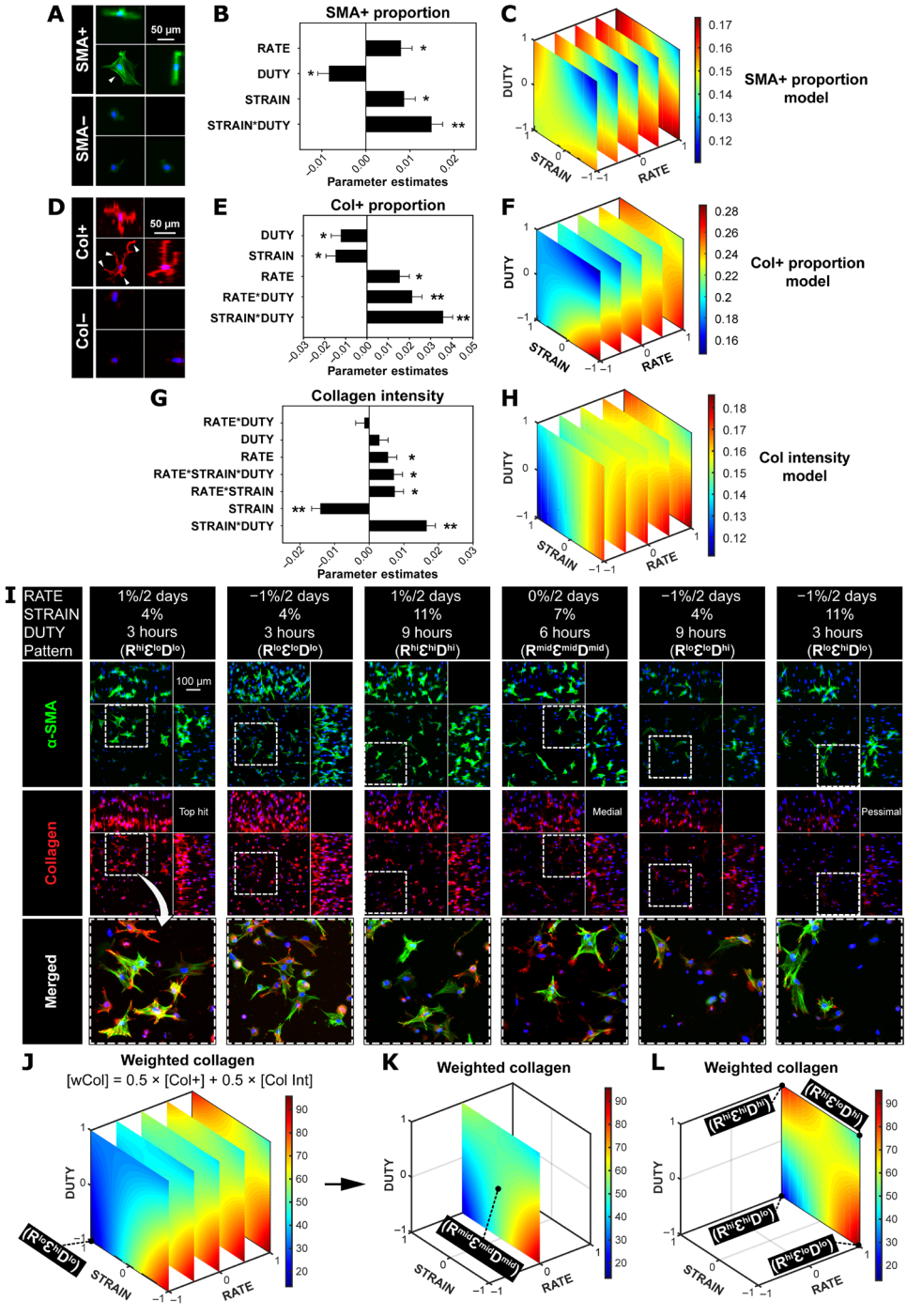

Fig. 2. Interaction between strain magnitude and duty period dominated MSC mechano-responsiveness. Parametric models of MSC responses for (**A** to **C**) the proportion of SMA+ cells, (**D** to **F**) proportion of Col+ cells, and (**G** and **H**) collagen mean intensity after 1 week of full factorial screening. (A) Example of a SMA+ cell with visible α-SMA stress fiber formation (top) (arrowhead) and a SMA− cell (bottom). SMA, green; nucleus, blue. (D) Example of a Col+ cell with visible collagen (in red) at the spreading cell protrusions and edges (top) (arrowheads) and a Col− cell (bottom). (B, E, and G) Summaries of factor effects (parameter estimates) for the proportion of SMA+ cells, proportion of Col+ cells, and collagen mean intensity. Larger coefficient magnitude of the parameter estimate corresponds to a larger effect of that factor on the model output. (C, F, and H) 4D response surface plot of the interaction between RATE, STRAIN, and DUTY on SMA+ proportion, Col+ proportion, and collagen mean intensity. The definition of the coded values is provided in table S1. (**I**) Representative maximum intensity projections of cells stained with α-SMA and collagen type I among various patterns of condition. Peripheral images are side view projections. Refer to table S2 for the polynomial models of SMA+ proportion, Col+ proportion, and collagen mean intensity. Error bars represent SE of the estimated parameters. $N = 3$ to 4 independent gels per condition. $^{**}P < 0.0001$ and $^{*}P < 0.05$. (**J** to **L**) The new metric weighted collagen (wCol) was defined to identify the top hit, medial, and pessimal conditions for further validation. Conditions selected are labeled on the graph and listed in table S3. (J) 4D response surface plot of the interaction between RATE, STRAIN, and DUTY on wCol. (K and L) Response surfaces of wCol with RATE at 0%/2 days (K) and at 1%/2 days (L).

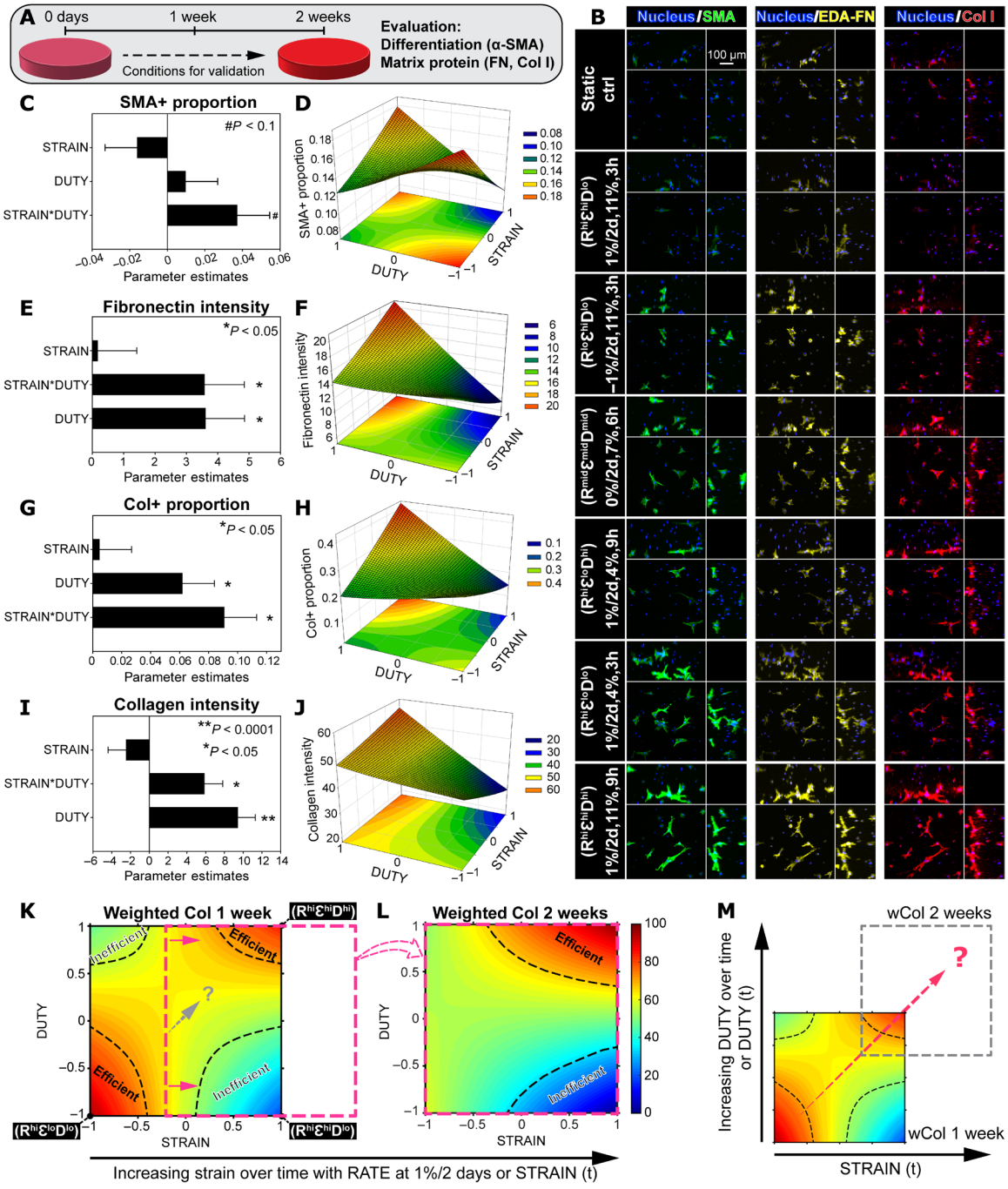

Fig. 3. Empirically driven model generated a hypothesis to enhance matrix production. (**A**) Overview of the 2-week validation culture of selected conditions. (**B**) Representative maximum intensity projections of MSCs stained with α-SMA, extra domain-A fibronectin (EDA-FN), and collagen type I. Peripheral images are side view projections. (**C** to **J**) Parametric analysis of MSC responses in expression of (C and D) α-SMA, (E and F) fibronectin, and (G to J) collagen with RATE at 1%/2 days. (C, E, G, and I) Summaries of factor effects (parameter estimation) for SMA+ cell proportion, fibronectin intensity, Col+ cell proportion, and collagen intensity, respectively. Error bars represent SE of the estimated parameters. $N = 3$ to 4 independent gels per condition. $^{**}P < 0.0001$, $^{*}P < 0.05$, and $\#P < 0.1$. (D, F, H, and J) Response surfaces of the STRAIN*DUTY interaction on SMA+ proportion, fibronectin intensity, Col+ proportion, and collagen intensity, respectively. 2D projections of the response surfaces are shown at the bottom in each plot. (**K**) Response surface of weighted collagen by 1 week with highlighted regions of efficient stimulation and inefficient stimulation (dashed outline) (RATE at 1%/2 days). (**L**) Response surface of wCol after 2 weeks of validation culture with regions of efficient and inefficient stimulation, shifted from that of 1 week in the direction of increasing STRAIN (pink arrows and outline). (**M**) Differences in response surfaces of wCol between 1 and 2 weeks, due to dynamic changes in the STRAIN*DUTY interaction effect, generated a hypothesis to optimally promote collagen production by MSCs (dashed arrow).

in most of the loading patterns tested when compared to those by 1 week (fig. S2, B and C). The strain magnitude*duty period interaction remained a positive and dominating effect after parametric analysis of collagen metrics including Col+ proportion, collagen intensity, normalized volume, and integrated density (Fig. 3, G and I; fig. S10, A and F; and table S4). Collagen production, measured by all the collagen metrics, peaked at high levels of strain magnitude and duty period and plunged with mismatched levels of strain magnitude and duty period [i.e., pattern ($R^{hi}\varepsilon^{hi}D^{hi}$) versus ($R^{hi}\varepsilon^{hi}D^{lo}$) in Fig. 3B and fig. S9; red versus blue in Fig. 3, H and J; figs. S8 and S10]. Evaluation of collagen production by wCol identified the pattern ($R^{hi}\varepsilon^{hi}D^{hi}$) that replaced the pattern ($R^{hi}\varepsilon^{lo}D^{lo}$) as the new top hit condition by 2 weeks (wCol = 100; figs. S5B and S6, right). This was due to more significant increases from 1 to 2 weeks in normalized Col+ proportion and collagen intensity of pattern ($R^{hi}\varepsilon^{hi}D^{hi}$) (1.9- to 9.3-fold and 1.2- to 2-fold, respectively) than those of pattern ($R^{hi}\varepsilon^{lo}D^{lo}$) (2.2- to 6.4-fold and 1.3- to 1.6-fold, respectively) (fig. S2, B and C). In addition, the pattern ($R^{hi}\varepsilon^{hi}D^{lo}$) replaced the pattern ($R^{lo}\varepsilon^{hi}D^{lo}$) as the new pessimal condition (wCol = 0; figs. S5B and S6, right), which showed little effect at promoting collagen production by 2 weeks (fig. S2, B and C).

*Increasing strain magnitude led to dynamic changes of strain magnitude*duty period interaction*

The above parametric analyses revealed that strain magnitude*duty period interaction but not individual strain magnitude or duty period was the dominant determinant of MSC mechanobiological responses, including the expression of α-SMA, fibronectin, and collagen. Comparison of the wCol response surfaces at high rate of strain change of 1%/2 days from the initial 1-week screening (Fig. 3K) and the 2-week validation (Fig. 3L) showed substantial differences. We categorized conditions with wCol > 75 as "efficient" to mark their promotive effect on high levels of collagen production and conditions with wCol < 50 as "inefficient" due to the little effect of mismatched levels of strain magnitude and duty period. After 2 weeks, patterns ($R^{hi}\varepsilon^{hi}D^{hi}$) (i.e., 1%/2 days, 11%, and 9 hours ON/OFF) and ($R^{hi}\varepsilon^{hi}D^{lo}$) (i.e., 1%/2 days, 11%, and 3 hours ON/OFF) remained in their respective categories of efficient and inefficient (Fig. 3, K and L), resulting in the new top hit and pessimal conditions. In comparison, the initial hit condition pattern ($R^{hi}\varepsilon^{lo}D^{lo}$) shifted out of its category of efficient with the new wCol only at medial levels (pink arrows and outline in Fig. 3K). This was due to the increasing strain magnitude (when rate of strain change was at 1%/2 days) from the initial 4 to 10% after 2 weeks of matching the unchanged duty period, thus causing dynamic changes in the effect of strain magnitude*duty period interaction from positive to negative [i.e., initially ($R^{hi}\varepsilon^{lo}D^{lo}$) to effectively ($R^{hi}\varepsilon^{hi}D^{lo}$) by 2 weeks]. Therefore, a reasonable deduction was that the initial hit condition ($R^{hi}\varepsilon^{lo}D^{lo}$) may outperform the new top hit condition ($R^{hi}\varepsilon^{hi}D^{hi}$) by 2 weeks, provided that the negative change of strain magnitude*duty period interaction can be mitigated. Collectively, this led us to hypothesize that increasing duty period to synchronize with increasing strain magnitude would yield a new condition that maintains the positive effect of strain magnitude*duty period interaction and consistently and efficiently promotes collagen production (dashed arrow in Fig. 3, K and M).

Synchronous application of strain magnitude and duty period promoted collagen production

To test our hypothesis, we repeated the 2-week culture and added a new condition pattern ($R^{hi}\varepsilon^{lo}D^{lo}$ sync) that matched the increasing strain magnitude to a stepwise increasing duty period (i.e., 3, 6, and 9 hours ON/OFF at days 2, 6, and 12, respectively). Compared to the original pattern ($R^{hi}\varepsilon^{lo}D^{lo}$) (Fig. 4A, left), the new pattern ($R^{hi}\varepsilon^{lo}D^{lo}$ sync) by design changed the strain magnitude and duty period from initially 4%, 3 hours to 7%, 6 hours after 1 week and to 10%, 9 hours after 2 weeks (Fig. 4A, right), thus maintaining the positive effect of strain magnitude*duty period. By analyzing both collagen and fibronectin, the results confirmed that the new pattern ($R^{hi}\varepsilon^{lo}D^{lo}$ sync) outperformed the previous conditions at promoting matrix production. Specifically, the pattern ($R^{hi}\varepsilon^{lo}D^{lo}$ sync) significantly and maximally promoted Col+ proportion and collagen intensity to 47.7 ± 1 and 24.2 ± 5%, respectively, compared to the previous hit conditions in the initial screen [i.e., pattern ($R^{hi}\varepsilon^{lo}D^{lo}$)] and in the validation culture [i.e., pattern ($R^{hi}\varepsilon^{hi}D^{hi}$)] (Fig. 4, B, C, and F, top). The corresponding wCol was also significantly higher for pattern ($R^{hi}\varepsilon^{lo}D^{lo}$ sync) than for patterns ($R^{hi}\varepsilon^{hi}D^{hi}$) and ($R^{hi}\varepsilon^{lo}D^{lo}$) (Fig. 4, D and F, top, and fig. S5C). Additional analysis of fibronectin also showed that the pattern ($R^{hi}\varepsilon^{lo}D^{lo}$ sync) significantly promoted fibronectin intensity by 60% compared to pattern ($R^{hi}\varepsilon^{lo}D^{lo}$), with marginal promotion compared to pattern ($R^{hi}\varepsilon^{hi}D^{hi}$) (Fig. 4, E and F, bottom). The loading patterns also had a significant effect on the cell density (fig. S4C), specifically with a close to twofold increase in the pattern ($R^{hi}\varepsilon^{lo}D^{lo}$ sync) compared to the control and the pattern ($R^{hi}\varepsilon^{lo}D^{lo}$).

DISCUSSION

Systematic and combinatorial studies are required for better understanding of mechanobiological cell responses to complex microenvironmental cues in engineered niches. However, predictive mechanobiological-based control of MSCs is still lacking largely because systematic investigations of dynamic mechanical stimulation protocols are not tractable with conventional experimental approaches and platforms. Full factorial screening with factors all at two levels is a common strategy used in the industrial experimentation for optimizing context-specific metrics (*14*, *35*, *36*). It requires relatively fewer runs compared to those with more levels per factor, thus probing factor effects more efficiently with finite resources. In this work, by using a 3D bioreactor array platform with combinatorial mechanical stimulation factors, we performed full factorial designs to evaluate the main effect of each factor and their higher-order interactions. With parametric modeling, we found that the interaction effect between strain magnitude and duty period of applied mechanical stimulation (STRAIN*DUTY) dominantly influenced myofibrogenesis and matrix production by MSCs. Furthermore, empirical modeling of higher-order interactions provided insights into the dynamic changes of strain magnitude*duty period interaction. These insights led us to hypothesize a new dynamic mechanical stimulation scheme in which strain magnitude and duty period were synchronously increased throughout the culture period. This approach was verified to outperform the original schemes in promoting MSC matrix production.

The parametric models were derived from empirical data to identify significant effects and hypothesis for validation, especially on collagen production (fig. S11). The parametric model fitting analyses of Col+ proportion and collagen intensity (fig. S11, B and C) both showed good fitting accuracy with low root mean square error (RMSE) (around $^1/_{10}$ of respective data mean) and no significant lack of fit for the regression models. The analysis of variance

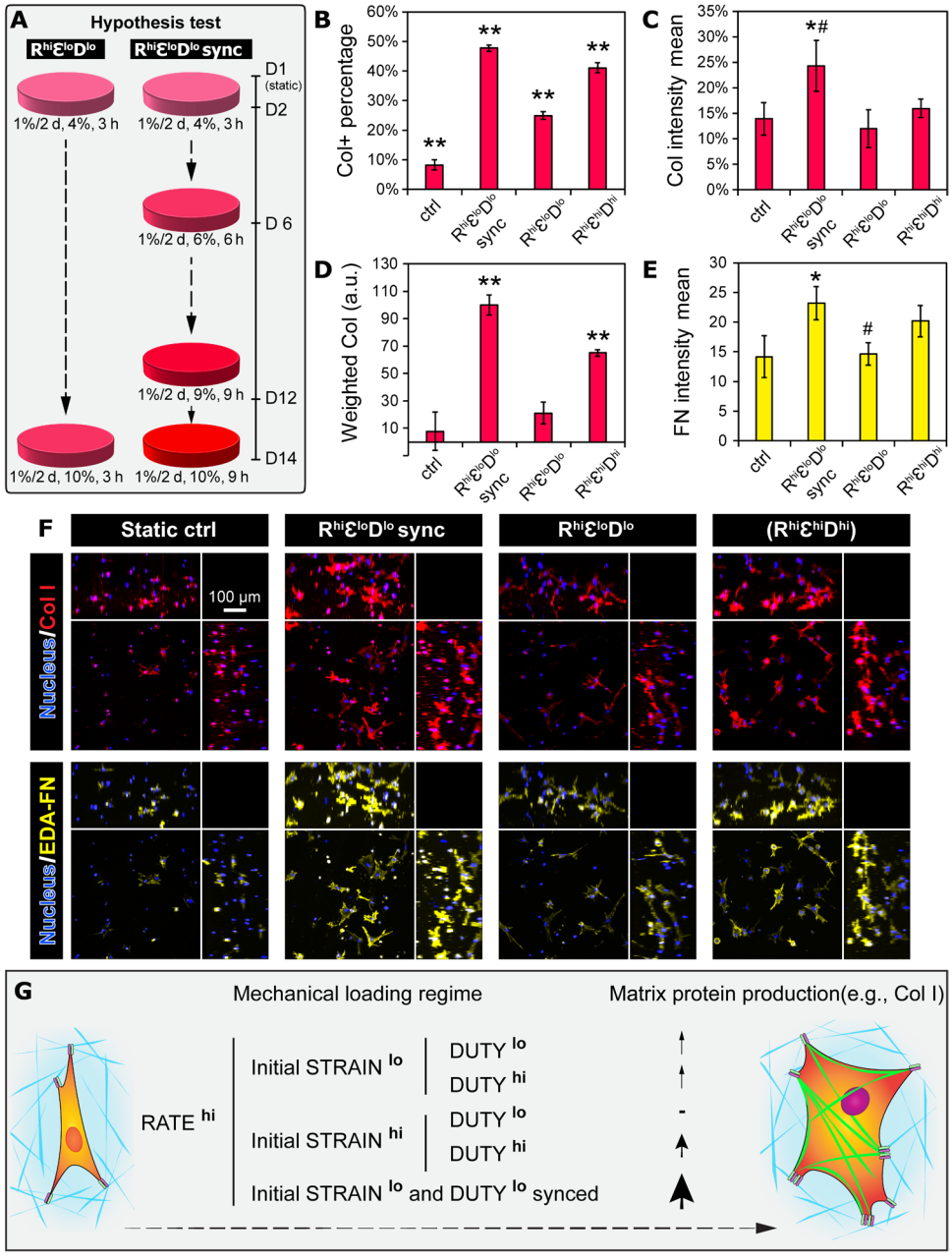

Fig. 4. Synchronous application of strain magnitude and duty period promoted collagen production. (**A**) Overview of the hypothesis test under the new condition for collagen and fibronectin production by MSCs. Left: The original pattern ($R^{hi}\varepsilon^{lo}D^{lo}$). Right: The new condition with dynamically synced STRAIN and DUTY, pattern ($R^{hi}\varepsilon^{lo}D^{lo}$ sync). (**B** to **E**) Quantification of collagen and fibronectin production using metrics including (B) Col+ proportion, (C) collagen intensity, (D) weighted collagen, and (E) fibronectin intensity. $N = 3$ to 4 independent gels per condition. $^{**}P < 0.01$ versus all other groups, $^{*}P < 0.05$ versus ctrl and pattern ($R^{hi}\varepsilon^{lo}D^{lo}$), and $\#P < 0.1$ versus pattern ($R^{hi}\varepsilon^{hi}D^{hi}$). (**F**) Representative maximum intensity projections of cells stained with collagen and ED-A FN from tested conditions. Peripheral images are side view projections. (**G**) Schematic summarizing the interplay between STRAIN and DUTY, possibly manifested through integrative regulation of force loading rate via molecular clutch and imprinted mechanical memory, which ultimately control the mechano-responsiveness of MSCs. a.u., arbitrary units.

(ANOVA) also indicated that the regression models and associated terms were the most significant source of variance instead of error ($P < 0.0001$ for both Col+ proportion and collagen intensity). Note that for SMA+ proportion (fig. S11A), a significant lack of fit was shown because of the center points not fitting into the current regression model. Nonetheless, the ANOVA showed that the regression model still had a significant effect at prediction beyond the center points ($P < 0.0001$, RMSE = 0.0166). The higher-order terms adopted in the parametric models only included interactive effects but not the quadratic (or higher-order) main factor effects (Supplementary Materials and Methods). Thus, the lack of fit of the center points strongly suggested a quadratic main effect or curvature effect. While the two-level full factorial design was best suited to probe the main factor effects and the interactive effects between

factors (*14*), additional levels for each factor (axial points) can be included to supplement the full factorial design and adopt quadratic main effect terms in the parametric model for better fitting and details of the curvature effects in future studies (*13*).

Our data showed that the individual effect of strain change rate (RATE) was consistently significant and positive. The application of an incremental strain (with positive rate of strain change at 1%/2 days) produced more α-SMA, fibronectin, and collagen (Fig. 2 and fig. S7). This is consistent with previous reports that showed increased collagen content per MSC-like cell in engineered constructs by incremental cyclic mechanical stimulation (*3*, *37*). It was previously shown that the benefit of constant "normal" mechanical stimulation gradually vanishes due to cell adaptation (*38*–*40*). The application of incremental strain (*41*, *42*) or resting/refractory periods (*43*–*45*) was believed to mitigate the cell adaptation by "resetting" the mechanosensitivity of cells and was shown to enhance cellular mechano-responses. Building on these earlier studies, our study revealed that the interaction effect between strain magnitude and duty period (STRAIN*DUTY) more dominantly regulated the mechano-responsiveness of MSCs compared to the individual effect of rate of strain change (or incremental strain alone) and duty period (or resting/duty OFF periods alone) (Fig. 2). The strain magnitude*duty period interaction can be observed even when the rate of strain change was at zero, which is the application of a constant strain stimulation (Fig. 2, C and K). This interaction effect is significant in that it not only reveals novel insights into new "keys" to control the mechano-responsiveness of MSCs for advanced bioprocess control and maturation of engineered tissues but also emphasizes the capability of using our approach to generate novel hypothesis for testing and validation.

The regulation of cell responses to stretching and related force transmission can be explained by the molecular clutch dynamics and the force loading rate, which is a fundamental factor driving the mechanosensitivity of the molecular clutch (*46*). Mechanical cues such as substrate rigidity and dynamic substrate stretching can directly regulate the force loading rate and influence several cell fate decisions and functions (*46*, *47*). Increasing strain at a constant stretching frequency (as in this study) or increasing frequency at a constant strain both convert to increasing force loading rate and transmission, similar to that acquired from increasing substrate rigidity. Individual mechanosensors in the clutch model experience these mechanical cues and also determine force transduction for downstream signaling (*46*). For instance, various levels of force loading rate induce rapid and/or long-term molecular events such as talin unfolding and integrin–extracellular matrix unbinding (*19*), adenosine triphosphate and other purinergic signaling, and gene silencing by chromatin compaction (*48*–*50*). Cyclic mechanical stretching and matrix stiffening have also been shown to modulate the activation of multiple transcription factors (*47*, *51*, *52*) and promote myofibroblast differentiation of MSC-like cells with SMA expression (*23*). Notably, we found significant difference between the expression pattern of SMA and collagen in terms of top hit conditions (Figs. 2 and 3 and fig. S2). This suggests discrepancy between myofibroblast differentiation of MSCs and their transformation into synthetic phenotype with optimal matrix production, where potential new insights could be generated using a similar approach to our study.

Mechanical cues including substrate rigidity and stretching have been shown to induce chromatin remodeling and influence the epigenomics of MSCs (*53*–*55*), although the specific mechanisms involved remain elusive. Mounting evidence supports the notion that repeated and lasting mechanical stimulation instills memory in stem cells including MSCs. Many mechanical priming-induced cellular events are differentially executed depending on culture history and have been proposed to serve as mechanical memory keepers on different levels, acting together to adjust the mechanosensitivity of MSCs to mechanical perturbation (*53*, *54*, *56*–*58*). For instance, the nuclear translocation of cotranscription factor Yes-associated protein (YAP) and chromatin condensation adapt rapidly to mechanical loading, but after loading cessation, YAP translocates back to the cytoplasm, and chromatin remodeling drops to baseline levels, resulting in reversible or weak mechanical memory and nominal changes in gene expression (*53*, *58*). In comparison, expression level of microRNA miR-21 was robust against acute changes in environmental mechanics due to long half-life of several days, serving as a long-term memory keeper (*57*). Higher magnitude of mechanical cues led to higher magnitude of mechanical memory imprinted in MSCs and extension of the permanency of memory and modulation on cell functions after loading cessation (*53*, *54*, *57*). Similarly, in our study, this mechanical memory may be differentially regulated depending on the level of strain magnitude and contribute to the strain magnitude*duty period interaction (Fig. 4G). For example, the patterns ($R^{hi}\varepsilon^{lo}D^{hi}$) and ($R^{hi}\varepsilon^{hi}D^{lo}$) may result in weak and strong memories, respectively, because of their respective strain levels and force transmission. These memories either do not persist through the high duty period and lead to only intermittent effect [i.e., ($R^{hi}\varepsilon^{lo}D^{hi}$)] or contribute to cell adaptation by lowering the mechanosensitivity of MSCs (*3*, *42*) and cause a diminishing effect [i.e., ($R^{hi}\varepsilon^{hi}D^{lo}$)], which are both suboptimal. Other patterns with positive strain magnitude*duty period interaction [i.e., ($R^{hi}\varepsilon^{lo}D^{lo}$) and ($R^{hi}\varepsilon^{hi}D^{hi}$)] seem to balance the mechanical memories and mechanosensitivity of MSCs and result in relatively more significant stimulating effects. Provided the dynamic nature of the imprinted memories due to increasing strain, we were led to hypothesize and demonstrate the strategy of maintaining the continuous and accumulative effects of stimulation for matrix production by matching increasing strain with increasing duty period (Fig. 4).

The goal of this study was not to reproduce the collagen content and organization of native load-bearing tissues but to increase the understanding of responses and development of engineered tissue constructs from MSCs to combinatorial and dynamic mechanical stimulation, specifically in terms of myofibrogenesis and matrix production. Myofibrogenesis may be more relevant to the engineering of specific tissues such as the heart valve and to specific disease modeling such as tissue fibrosis. More comprehensive biological analysis can be performed for context-specific applications when needed. The strategy of integrating microdevice arrays and parametric modeling to identify the combinatorial and specific effects of mechanical stimulation can be widely applied to other cell sources (e.g., vascular smooth muscle cell) (*1*, *19*). Other factors of interest can also be included such as fluidic shear stress, scaffold materials, and media formulations for combinatorial screening of their high-order effects on engineered (load-bearing) tissue formation and functions. Note that fluidic shear stress is also a potent mechanical stimulus for modulating MSC fate and functions (*6*, *59*). While not explicitly characterized and examined in this study, interstitial flow induced by cyclic deformation of the gels may have contributed to the observed cell responses. We performed offline mechanical compression testing to characterize the mechanical properties of

the gels and observed no significant differences of gel compressive modulus across the loading patterns (fig. S12), regardless of differential collagen expression. This indicated that the cross-linked hydrogel was still the dominant mechanical structure and that the amount of collagen produced was not significant enough to influence the stiffness of the bulk gel or the straining pattern as designed. In comparison, noninvasive functional analysis on chip, similar to integrating strain sensors to monitor the stiffness evolution of engineered constructs (*60*), would be revolutionary at providing new insights into the dynamics of tissue development. Moreover, the PEG-NB hydrogel system permits precise definition of material and biochemical cues (*13*), and similar combinatorial screening studies can be implemented to understand the specific and integrative effects of critical microenvironmental factors, leading to comprehensive mechanobiology of target cell niches that can serve as a basis for designing next-generation biomaterials.

This paper reported a combinatorial screening study of the individual and integrative effects of 3D dynamic mechanical stimulation parameters on myofibrogenesis and matrix production by MSCs cultured in 3D hydrogel constructs. Our deformable membrane microdevice arrays were paired effectively with combinatorial experimental design and parametric regression modeling to generate insights otherwise not available. Notably, a high-order and significant strain magnitude*duty period interaction effect was found that dominantly determined myofibrogenesis and matrix production by MSCs. A novel dynamic loading regime was predicted on the basis of empirically driven models to promote matrix production by MSCs through optimizing their mechano-responsiveness. The optimal regime predicted by our study—pattern ($R^{hi}\varepsilon^{lo}D^{lo}$ sync) where strain magnitude and duty period were synchronously increased over time—was validated to most effectively promote collagen and fibronectin production. Our findings inform the design of efficient mechanical loading regimes for MSC-based tissue regeneration. They also represent a clearly generalizable approach to probe multifactorial regulation of cell fate by combinatorially controlling microenvironmental stimuli.

MATERIALS AND METHODS

Please refer to the Supplementary Materials for detailed methods and data analysis.

Device fabrication and integration of PEG-NB gel array

The deformable membrane microdevice array is based on our previously developed platform (*60*, *61*). Dynamic 3D mechanical stretching was successfully applied to the PEG-NB hydrogel arrays by covalently bonding them to the membrane, which is pneumatically actuated. PEG-NB hydrogel system was used for 3D culture of MSCs because its biochemical and material properties are tunable, including adhesion peptide identities and densities, elasticity, and degradability (*13*, *61*).

Human MSC culture

Cryopreserved human bone marrow–derived MSCs were obtained from the Texas A&M Health Science Center, College of Medicine Institute for Regenerative Medicine at Scott & White through a grant from the National Center for Research Resources of the National Institutes of Health (grant no. P40RR017447). MSCs at passages 4 to 5 and complete culture medium containing 81.7% α–minimum essential medium with L-glutamine, 16.3% fetal bovine serum, 1% additional L-glutamine, and 1% penicillin/streptomycin were used for all experiments.

Finite element analysis

3D finite element simulations of the bulging membrane-gel system were performed using ANSYS Workbench v14.0 (ANSYS Inc., Canonsburg, PA) to determine the pressure needed for pneumatic actuation to achieve the prescribed strain magnitude.

Immunofluorescence staining

Myofibroblast differentiation is defined with neo-expression and incorporation of α-SMA into stress fibers (*31*). Therefore, single-cell immunofluorescence-based analysis is appropriate to identify the proportion of myofibroblasts from a population of cells. Expression of ED-A (extra domain-A) fibronectin precedes, is necessary for myofibroblast activation, and is suggested to serve as master template for collagen deposition (*32*, *34*, *62*). MSCs embedded in the PEG-NB gels were stained for α-SMA with fluorescein isothiocyanate–conjugated mouse monoclonal anti-human α-SMA (F3777, Sigma-Aldrich; dilution 1:300), cellular ED-A fibronectin with mouse monoclonal anti–ED-A fibronectin (IST-9, sc-59826, Santa Cruz Biotechnology; dilution 1:200), and collagen with rabbit monoclonal anti–collagen type I (ab138492, Abcam; dilution 1:300).

Confocal microscopy imaging and analysis

A laser scanning confocal microscope (Zeiss LSM710) with a 20× objective (Plan-Apochromat 20×/1.0 DIC, water immersion) was used to acquire optical slices of the 3D hydrogel constructs. Imaris (Bitplane) was used to create automatically thresholded, quantifiable 3D surfaces around stained objects in the hydrogels for each laser channel from confocal image stacks. To comprehensively assess the collagen production from all cells, a new metric weighted collagen was defined on the basis of Col+ proportion and collagen intensity. Each condition was graded and ranked for both Col+ proportion [Col+] and collagen intensity [Col Int], proportionally with the highest value to 100 and lowest to 0. The weighted collagen [wCol] was defined using an objective function with weighted Col+ proportion and weighted collagen intensity. The sensitivity of [wCol] to different weight assignment (i.e., 0.25:0.75, 0.5:0.5, and 0.75:0.25 for [Col+]:[Col Int]) was tested for all the experiments involving the analysis of weighted collagen.

Factorial design of experiments and statistical analysis

The approach of two-level full factorial design of experiments was applied to estimate and probe the significance of all individual main effects and interaction effects of factors (i.e., parameters of dynamic mechanical stimulation—rate of strain change or RATE, initial strain magnitude or STRAIN, and duty period or DUTY) on a given output metric (e.g., α-SMA, collagen, or fibronectin expression) (*14*, *35*). A two-level full factorial design included experimental runs at every possible combination of high and low levels of interest for each factor (eight runs in total) (i.e., rate of strain change from 1%/2 days to −1%/2 days, strain magnitude from 11 to 4%, and duty period with 50% duty cycle from 9 hours ON/9 hours OFF to 3 hours ON/3 hours OFF; Fig. 1B and table S1). Additional combinations involving medial levels of factors or "center points" were replicated and included to estimate the pure error for probing the significance of all the effects and to detect potential quadratic or curvature

effects (i.e., rate of strain change at 0%/2 days, strain magnitude at 7%, and duty period at 6 hours ON/6 hours OFF; table S1). The conditions of the three-factor full factorial design were randomized in experiments, with each combination of factors imposed to at least three replicated gels to increase the statistical power and accuracy for parametric modeling. Table S3 lists the minimal number of combinations required to estimate and probe the significance of all the effects in the two-factor, two-level full factorial design (i.e., assessing only factors of STRAIN and DUTY). All listed combinations were performed with at least three replicated gels (table S3). Parametric models were generated on the combinatorial cue-response data, and associated statistical analysis was performed all using JMP® v13 (SAS Institute). Additional statistical analyses were performed using SigmaPlot 12. Data are reported as means ± SEM unless otherwise noted and were analyzed by one- and two-way ANOVA with Tukey post hoc tests for all pairwise comparisons and with statistical significance evaluated at $P < 0.05$.

Parametric modeling

In a process as described previously (*12*, *14*), response surfaces were modeled by linear regression. For example, for a three-factor response surface, the output response (Y) was modeled as a function of independent input factors (X_i) in a polynomial function Eq. 1

$$Y = K + \beta_1 X_1 + \beta_2 X_2 + \beta_3 X_3 + \beta_{12} X_1 X_2 + \beta_{13} X_1 X_3 + \beta_{23} X_2 X_3 + \beta_{123} X_1 X_2 X_3 \quad (1)$$

where K corresponds to the average response of center points, β_i the main effect coefficients, and β_{ij} the second-order interaction coefficients. The design matrix and coded values are described in table S1. Coded values were useful as they allow for the determination of factor effects independent of units through the comparison of β coefficients (*35*). Model parameters were estimated using least squares estimation in JMP, and the statistical significance of each parameter was evaluated at $P < 0.05$. Insignificant factors were removed from the initial model by rank, and model parameters were calculated for the reduced model through an iterative process of backward elimination (*12*).

SUPPLEMENTARY MATERIALS

Supplementary material for this article is available at http://advances.sciencemag.org/cgi/content/full/7/19/eabe7204/DC1

View/request a protocol for this paper from *Bio-protocol*.

REFERENCES AND NOTES

1. G. C. Engelmayr Jr., V. L. Sales, J. E. Mayer, M. S. Sacks, Cyclic flexure and laminar flow synergistically accelerate mesenchymal stem cell-mediated engineered tissue formation: Implications for engineered heart valve tissues. *Biomaterials* **27**, 6083–6095 (2006).
2. A. L. Y. Nachlas, S. Li, B. W. Streeter, K. J. de Jesus Morales, F. Sulejmani, D. I. Madukauwa-David, D. Bejleri, W. Sun, A. P. Yoganathan, M. E. Davis, A multilayered valve leaflet promotes cell-laden collagen type I production and aortic valve hemodynamics. *Biomaterials* **240**, 119838 (2020).
3. Z. H. Syedain, J. S. Weinberg, R. T. Tranquillo, Cyclic distension of fibrin-based tissue constructs: Evidence of adaptation during growth of engineered connective tissue. *Proc. Natl. Acad. Sci. U.S.A.* **105**, 6537–6542 (2008).
4. B. S. Kim, J. Nikolovski, J. Bonadio, D. J. Mooney, Cyclic mechanical strain regulates the development of engineered smooth muscle tissue. *Nat. Biotechnol.* **17**, 979–983 (1999).
5. N. Y. Liaw, W. H. Zimmermann, Mechanical stimulation in the engineering of heart muscle. *Adv. Drug Deliv. Rev.* **96**, 156–160 (2016).
6. L. MacQueen, Y. Sun, C. A. Simmons, Mesenchymal stem cell mechanobiology and emerging experimental platforms. *J. R. Soc. Interface* **10**, –20130179 (2013).
7. A. Uccelli, L. Moretta, V. Pistoia, Mesenchymal stem cells in health and disease. *Nat. Rev. Immunol.* **8**, 726–736 (2008).
8. S. Ramaswamy, D. Gottlieb, G. C. Engelmayr Jr., E. Aikawa, D. E. Schmidt, D. M. Gaitan-Leon, V. L. Sales, J. E. Mayer Jr., M. S. Sacks, The role of organ level conditioning on the promotion of engineered heart valve tissue development in-vitro using mesenchymal stem cells. *Biomaterials* **31**, 1114–1125 (2010).
9. J. Seo, J.-Y. Shin, J. Leijten, O. Jeon, G. Camci-Unal, A. D. Dikina, K. Brinegar, A. M. Ghaemmaghami, E. Alsberg, A. Khademhosseini, High-throughput approaches for screening and analysis of cell behaviors. *Biomaterials* **153**, 85–101 (2017).
10. C. Moraes, Y. Sun, C. A. Simmons, (Micro)managing the mechanical microenvironment. *Integr. Biol.* **3**, 959–971 (2011).
11. E. H. Nguyen, M. R. Zanotelli, M. P. Schwartz, W. L. Murphy, Differential effects of cell adhesion, modulus and VEGFR-2 inhibition on capillary network formation in synthetic hydrogel arrays. *Biomaterials* **35**, 2149–2161 (2014).
12. W. L. K. Chen, M. Likhitpanichkul, A. Ho, C. A. Simmons, Integration of statistical modeling and high-content microscopy to systematically investigate cell-substrate interactions. *Biomaterials* **31**, 2489–2497 (2010).
13. J. Usprech, D. A. Romero, C. H. Amon, C. A. Simmons, Combinatorial screening of 3D biomaterial properties that promote myofibrogenesis for mesenchymal stromal cell-based heart valve tissue engineering. *Acta Biomater.* **58**, 34–43 (2017).
14. R. G. Ireland, M. Kibschull, J. Audet, M. Ezzo, B. Hinz, S. J. Lye, C. A. Simmons, Combinatorial extracellular matrix microarray identifies novel bioengineered substrates for xeno-free culture of human pluripotent stem cells. *Biomaterials* **248**, 120017 (2020).
15. C.-H. Ku, P. H. Johnson, P. Batten, P. Sarathchandra, R. C. Chambers, P. M. Taylor, M. H. Yacoub, A. H. Chester, Collagen synthesis by mesenchymal stem cells and aortic valve interstitial cells in response to mechanical stretch. *Cardiovasc. Res.* **71**, 548–556 (2006).
16. J. Usprech, W. L. K. Chen, C. A. Simmons, Heart valve regeneration: The need for systems approaches. *Wiley Interdiscip. Rev. Syst. Biol. Med.* **8**, 169–182 (2016).
17. M. P. Rubbens, A. Mol, R. A. Boerboom, R. A. Bank, F. P. T. Baaijens, C. V. C. Bouten, Intermittent straining accelerates the development of tissue properties in engineered heart valve tissue. *Tissue Eng. Part A* **15**, 999–1008 (2009).
18. J. Z. Paxton, P. Hagerty, J. J. Andrick, K. Baar, Optimizing an intermittent stretch paradigm using ERK1/2 phosphorylation results in increased collagen synthesis in engineered ligaments. *Tissue Eng. Part A* **18**, 277–284 (2012).
19. G. C. Engelmayr, E. Rabkin, F. W. H. Sutherland, F. J. Schoen, J. E. Mayer, M. S. Sacks, The independent role of cyclic flexure in the early in vitro development of an engineered heart valve tissue. *Biomaterials* **26**, 175–187 (2005).
20. C. J. Flaim, D. Teng, S. Chien, S. N. Bhatia, Combinatorial signaling microenvironments for studying stem cell fate. *Stem Cells Dev.* **17**, 29–39 (2008).
21. S. Gobaa, S. Hoehnel, M. Roccio, A. Negro, S. Kobel, M. P. Lutolf, Artificial niche microarrays for probing single stem cell fate in high throughput. *Nat. Methods* **8**, 949–955 (2011).
22. S. L. Vega, M. Y. Kwon, K. H. Song, C. Wang, R. L. Mauck, L. Han, J. A. Burdick, Combinatorial hydrogels with biochemical gradients for screening 3D cellular microenvironments. *Nat. Commun.* **9**, 614 (2018).
23. C. Moraes, M. Likhitpanichkul, C. J. Lam, B. M. Beca, Y. Sun, C. A. Simmons, Microdevice array-based identification of distinct mechanobiological response profiles in layer-specific valve interstitial cells. *Integr. Biol.* **5**, 673–680 (2013).
24. Y. Kamotani, T. Bersano-Begey, N. Kato, Y. C. Tung, D. Huh, J. W. Song, S. Takayama, Individually programmable cell stretching microwell arrays actuated by a Braille display. *Biomaterials* **29**, 2646–2655 (2008).
25. L. MacQueen, O. Chebotarev, C. A. Simmons, Y. Sun, Miniaturized platform with on-chip strain sensors for compression testing of arrayed materials. *Lab Chip* **12**, 4178–4184 (2012).
26. C. Moraes, G. Wang, Y. Sun, C. A. Simmons, A microfabricated platform for high-throughput unconfined compression of micropatterned biomaterial arrays. *Biomaterials* **31**, 577–584 (2010).
27. K. Sakthivel, H. Kumar, M. G. A. Mohamed, B. Talebjedi, J. Shim, H. Najjaran, M. Hoorfar, K. Kim, High throughput screening of cell mechanical response using a stretchable 3D cellular microarray platform. *Small* **16**, 2000941 (2020).
28. E. Rabkin-Aikawa, M. Farber, M. Aikawa, F. J. Schoen, Dynamic and reversible changes of interstitial cell phenotype during remodeling of cardiac valves. *J. Heart Valve Dis.* **13**, 841–847 (2004).
29. E. Aikawa, P. Whittaker, M. Farber, K. Mendelson, R. F. Padera, M. Aikawa, F. J. Schoen, Human semilunar cardiac valve remodeling by activated cells from fetus to adult: Implications for postnatal adaptation, pathology, and tissue engineering. *Circulation* **113**, 1344–1352 (2006).
30. M. Walraven, B. Hinz, Therapeutic approaches to control tissue repair and fibrosis: Extracellular matrix as a game changer. *Matrix Biol.* **71–72**, 205–224 (2018).
31. J. J. Tomasek, G. Gabbiani, B. Hinz, C. Chaponnier, R. A. Brown, Myofibroblasts and mechano-regulation of connective tissue remodelling. *Nat. Rev. Mol. Cell Biol.* **3**, 349–363 (2002).

32. F. Klingberg, G. Chau, M. Walraven, S. Boo, A. Koehler, M. L. Chow, A. L. Olsen, M. Im, M. Lodyga, R. G. Wells, E. S. White, B. Hinz, The fibronectin ED-A domain enhances recruitment of latent TGF-β-binding protein-1 to the fibroblast matrix. *J. Cell Sci.* **131**, jcs201293 (2018).
33. M. Kohan, A. F. Muro, E. S. White, N. Berkman, EDA-containing cellular fibronectin induces fibroblast differentiation through binding to α4β7 integrin receptor and MAPK/Erk 1/2-dependent signaling. *FASEB J.* **24**, 4503–4512 (2010).
34. A. F. Muro, F. A. Moretti, B. B. Moore, M. Yan, R. G. Atrasz, C. A. Wilke, K. R. Flaherty, F. J. Martinez, J. L. Tsui, D. Sheppard, F. E. Baralle, G. B. Toews, E. S. White, An essential role for fibronectin extra type III domain A in pulmonary fibrosis. *Am. J. Respir. Crit. Care Med.* **177**, 638–645 (2008).
35. D. C. Montgomery, *Design and Analysis of Experiments* (John Wiley & Sons Inc, ed. 9, 2017).
36. M. Krzywinski, N. Altman, Points of significance: Two-factor designs. *Nat. Methods* **11**, 1187–1188 (2014).
37. Z. H. Syedain, R. T. Tranquillo, Controlled cyclic stretch bioreactor for tissue-engineered heart valves. *Biomaterials* **30**, 4078–4084 (2009).
38. L. E. Lanyon, The success and failure of the adaptive response to functional load-bearing in averting bone fracture. *Bone* **13** (suppl. 2), S17–S21 (1992).
39. C. H. Turner, Three rules for bone adaptation to mechanical stimuli. *Bone* **23**, 399–407 (1998).
40. T. Watanabe-Nakayama, S. I. Machida, I. Harada, H. Sekiguchi, R. Afrin, A. Ikai, Direct detection of cellular adaptation to local cyclic stretching at the single cell level by atomic force microscopy. *Biophys. J.* **100**, 564–572 (2011).
41. Z. H. Syedain, R. T. Tranquillo, TGF-β1 diminishes collagen production during long-term cyclic stretching of engineered connective tissue: Implication of decreased ERK signaling. *J. Biomech.* **44**, 848–855 (2011).
42. J. S. Weinbaum, J. B. Schmidt, R. T. Tranquillo, Combating adaptation to cyclic stretching by prolonging activation of extracellular signal-regulated kinase. *Cell. Mol. Bioeng.* **6**, 279–286 (2013).
43. N. A. Plunkett, S. Partap, F. J. O'Brien, Osteoblast response to rest periods during bioreactor culture of collagen-glycosaminoglycan scaffolds. *Tissue Eng. Part A* **16**, 943–951 (2010).
44. B. Sen, Z. Xie, N. Case, M. Styner, C. T. Rubin, J. Rubin, Mechanical signal influence on mesenchymal stem cell fate is enhanced by incorporation of refractory periods into the loading regimen. *J. Biomech.* **44**, 593–599 (2011).
45. G. M. Pagnotti, M. Styner, G. Uzer, V. S. Patel, L. E. Wright, K. K. Ness, T. A. Guise, J. Rubin, C. T. Rubin, Combating osteoporosis and obesity with exercise: Leveraging cell mechanosensitivity. *Nat. Rev. Endocrinol.* **15**, 339–355 (2019).
46. A. Elosegui-Artola, X. Trepat, P. Roca-Cusachs, Control of mechanotransduction by molecular clutch dynamics. *Trends Cell Biol.* **28**, 356–367 (2018).
47. Y. Cui, F. M. Hameed, B. Yang, K. Lee, C. Q. Pan, S. Park, M. Sheetz, Cyclic stretching of soft substrates induces spreading and growth. *Nat. Commun.* **6**, 6333 (2015).
48. J. Gardinier, W. Yang, G. R. Madden, A. Kronbergs, V. Gangadharan, E. Adams, K. Czymmek, R. L. Duncan, $P2Y_2$ receptors regulate osteoblast mechanosensitivity during fluid flow. *Am. J. Physiol. Cell Physiol.* **306**, C1058–C1067 (2014).
49. D. C. Genetos, D. J. Geist, D. Liu, H. J. Donahue, R. L. Duncan, Fluid shear-induced ATP secretion mediates prostaglandin release in MC3T3-E1 osteoblasts. *J. Bone Miner. Res.* **20**, 41–49 (2005).
50. D. Nicetto, G. Donahue, T. Jain, T. Peng, S. Sidoli, L. Sheng, T. Montavon, J. S. Becker, J. M. Grindheim, K. Blahnik, B. A. Garcia, K. Tan, R. Bonasio, T. Jenuwein, K. S. Zaret, H3K9me3-heterochromatin loss at protein-coding genes enables developmental lineage specification. *Science* **363**, 294–297 (2019).
51. X. Huang, N. Yang, V. F. Fiore, T. H. Barker, Y. Sun, S. W. Morris, Q. Ding, V. J. Thannickal, Y. Zhou, Matrix stiffness-induced myofibroblast differentiation is mediated by intrinsic mechanotransduction. *Am. J. Respir. Cell Mol. Biol.* **47**, 340–348 (2012).
52. A. Elosegui-artola, I. Andreu, A. E. M. Beedle, A. Lezamiz, M. Uroz, A. J. Kosmalska, R. Oria, J. Z. Kechagia, P. Rico-Lastres, A.-L. Le Roux, C. M. Shanahan, X. Trepat, D. Navajas, S. Garcia-Manyes, P. Roca-Cusachs, Force triggers YAP nuclear entry by regulating transport across nuclear pores. *Cell* **171**, 1397–1410.e14 (2017).
53. S.-J. Heo, S. D. Thorpe, T. P. Driscoll, R. L. Duncan, D. A. Lee, R. L. Mauck, Biophysical regulation of chromatin architecture instills a mechanical memory in mesenchymal stem cells. *Sci. Rep.* **5**, 16895 (2015).
54. S. J. Heo, W. M. Han, S. E. Szczesny, B. D. Cosgrove, D. M. Elliott, D. A. Lee, R. L. Duncan, R. L. Mauck, Mechanically induced chromatin condensation requires cellular contractility in mesenchymal stem cells. *Biophys. J.* **111**, 864–874 (2016).
55. N. Jain, K. V. Iyer, A. Kumar, G. V. Shivashankar, Cell geometric constraints induce modular gene-expression patterns via redistribution of HDAC3 regulated by actomyosin contractility. *Proc. Natl. Acad. Sci. U.S.A.* **110**, 11349–11354 (2013).
56. C. Yang, M. W. Tibbitt, L. Basta, K. S. Anseth, Mechanical memory and dosing influence stem cell fate. *Nat. Mater.* **13**, 645–652 (2014).
57. C. X. Li, N. P. Talele, S. Boo, A. Koehler, E. Knee-Walden, J. L. Balestrini, P. Speight, A. Kapus, B. Hinz, MicroRNA-21 preserves the fibrotic mechanical memory of mesenchymal stem cells. *Nat. Mater.* **16**, 379–389 (2016).
58. A. R. Killaars, J. C. Grim, C. J. Walker, E. A. Hushka, T. E. Brown, K. S. Anseth, Extended exposure to stiff microenvironments leads to persistent chromatin remodeling in human mesenchymal stem cells. *Adv. Sci.* **6**, 1801483 (2018).
59. E. J. Arnsdorf, P. Tummala, R. Y. Kwon, C. R. Jacobs, Mechanically induced osteogenic differentiation - The role of RhoA, ROCKII and cytoskeletal dynamics. *J. Cell Sci.* **122**, 546–553 (2009).
60. H. Liu, L. A. MacQueen, J. F. Usprech, H. Maleki, K. L. Sider, M. G. Doyle, Y. Sun, C. A. Simmons, Microdevice arrays with strain sensors for 3D mechanical stimulation and monitoring of engineered tissues. *Biomaterials* **172**, 30–40 (2018).
61. H. Liu, J. Usprech, Y. Sun, C. A. Simmons, A microfabricated platform with hydrogel arrays for 3D mechanical stimulation of cells. *Acta Biomater.* **34**, 113–124 (2016).
62. F. Klingberg, M. L. Chow, A. Koehler, S. Boo, L. Buscemi, T. M. Quinn, M. Costell, B. A. Alman, E. Genot, B. Hinz, Prestress in the extracellular matrix sensitizes latent TGF-β1 for activation. *J. Cell Biol.* **207**, 283–297 (2014).

Acknowledgments: We acknowledge the AOMF for the use of confocal microscopy for imaging and the Imaris software for data analysis. **Funding:** We acknowledge financial support from the Canadian Institutes of Health Research (CIHR) Operating Grant (MOP-130481), the Ontario Research Fund–Research Excellence program, and Canada Research Chair in Mechanobiology to C.A.S. and Micro and Nanoengineering Systems to Y.S. **Author contributions:** H.L.: Conceptualization, methodology, investigation, data analysis and presentation, and writing—original draft and revision. J.F.U.: Methodology, investigation, and writing—review and editing. P.K.P.: Investigation. Y.S.: Supervision, methodology, funding acquisition, and writing—review and editing. C.A.S.: Conceptualization, methodology, writing—review and editing, funding acquisition, supervision, and project administration. **Competing interests:** The authors declare that they have no competing interests. **Data and materials availability:** All data needed to evaluate the conclusions in the paper are present in the paper and/or the Supplementary Materials. Additional data related to this paper may be requested from the authors.

Submitted 14 September 2020
Accepted 19 March 2021
Published 7 May 2021
10.1126/sciadv.abe7204

Citation: H. Liu, J. F. Usprech, P. K. Parameshwar, Y. Sun, C. A. Simmons, Combinatorial screen of dynamic mechanical stimuli for predictive control of MSC mechano-responsiveness. *Sci. Adv.* **7**, eabe7204 (2021).

Science Advances

Combinatorial screen of dynamic mechanical stimuli for predictive control of MSC mechano-responsiveness

Haijiao Liu, Jenna F. Usprech, Prabu Karthick Parameshwar, Yu Sun and Craig A. Simmons

Sci Adv **7** (19), eabe7204.
DOI: 10.1126/sciadv.abe7204

Science Advances (ISSN 2375-2548) is published by the American Association for the Advancement of Science, 1200 New York Avenue NW, Washington, DC 20005. The title *Science Advances* is a registered trademark of AAAS.